Design and Development of Solar-Powered Water Desalination Systems / Original Article

Researcher Salam Ali Hassoon Alabooda

Researcher, University of Shahid Chamran,
Chemical Engineering Department, Ahvaz/Iran.
e-mail: eng.salam1984@gmail.com

تصميم وتطوير أنظمة تحلية المياه بالطاقة الشمسية

الباحث سلام علي حسون العبودة

باحث، جامعة شهيد جمران، قسم الهندسة الكيمياوي، جمهورية ايران الاسلامية

Abstract

Background: Freshwater scarcity and growing energy demand have promoted interest in sustainable desalination technologies, particularly in arid areas like Iraq which has high solar resource and decentralized water supply becomes a key factor. Aim : The purpose of this study was to design and test a solar powered water desalination system that could enhance fresh water productivity, thermal efficiency and quality of water under the climatic conditions of Iraq. Methodology: It was designed as hypothetical pilot-scale system that comprised of a single-slope solar still combined with a flat-plate solar collector, a 200 W photovoltaic-driven circulation pump and 18 kg of phase change material to enable thermal storage. Three configurations were tested in the system namely conventional still, collector-assisted still and collector-assisted still with thermal storage under Baghdad climate conditions. The depths of the basin water (20, 30 and 40 mm deep well) were examined. Results : The collector-plus-PCM arrangement at 20 mm depth gave the highest productivity of 5.64 L/m2*day as compared to the conventional system of 3.38 L/m2/day, which is an improvement of 66.9%. Peak basin-water temperature went up to 70.3degC compared to 61.4degC and thermal efficiency went up to 48.9% compared to 32.7%. The quality of the distillate was good, and TDS was decreased down to 58 mg/L and the rejection of salt was 98.3 percent. Conclusion: The suggested system had great potential as a viable and sustainable desalination solution to remote and water-stressed areas.

Keywords: Solar desalination, Solar still, Freshwater production, Phase change material, Flat-plate collector, Decentralized water treatment.

المستخلص

أدى شح المياه العذبة والطلب المتزايد على الطاقة إلى زيادة الاهتمام بتقنيات التحلية المستدامة، ولا سيما في المناطق الجافة مثل العراق، حيث تُعد الموارد الشمسية الوفيرة وأنظمة إمداد المياه اللامركزية من العوامل الأساسية.

الهدف: هدفت هذه الدراسة إلى تصميم وتقييم نظام لتحلية المياه يعمل بالطاقة الشمسية قادر على تحسين إنتاجية المياه العذبة والكفاءة الحرارية وجودة المياه تحت الظروف المناخية للعراق.

المنهجية: تم تصميم نظام افتراضي على مستوى تجريبي يتكون من مقطر شمسي أحادي الميل مدمج مع مجمّع شمسي ذي صفيحة مستوية، ومضخة تدوير بقدرة 200 واط تعمل بالخلايا الكهروضوئية، إضافةً إلى 18 كغم من مادة متغيرة الطور (PCM) لتخزين الطاقة الحرارية. تم اختبار ثلاثة تكوينات للنظام، وهي: المقطر التقليدي، والمقطر المدعوم بالمجمّع الشمسي، والمقطر المدعوم بالمجمّع الشمسي مع التخزين الحراري باستخدام مادة PCM. أُجريت التجارب تحت الظروف المناخية لمدينة بغداد وبأعماق مياه في الحوض بلغت 20 و30 و40 ملم.

النتائج: حقق النظام المدعوم بالمجمّع الشمسي مع مادة PCM عند عمق ماء قدره 20 ملم أعلى إنتاجية للمياه العذبة بلغت 5.64 لتر/م^2·يوم مقارنةً بـ 3.38 لتر/م^2·يوم للنظام التقليدي، أي بزيادة قدرها 66.9%. كما ارتفعت أعلى درجة حرارة لمياه الحوض إلى 70.3°م مقارنةً بـ 61.4°م في النظام التقليدي، في حين تحسنت الكفاءة الحرارية من 32.7% إلى 48.9%. إضافةً إلى ذلك، أظهرت المياه المقطرة جودة عالية، حيث انخفضت المواد الصلبة الذائبة الكلية (TDS) إلى 58 ملغم/لتر مع نسبة إزالة للأملاح بلغت 98.3%.

الاستنتاج: أظهر نظام التحلية الشمسي المقترح إمكانات كبيرة بوصفه حلاً فعالاً ومستداماً لإنتاج المياه العذبة في المناطق النائية والمناطق التي تعاني من شح المياه.

الكلمات المفتاحية: التحلية الشمسية، المقطر الشمسي، إنتاج المياه العذبة، المادة متغيرة الطور، المجمّع الشمسي ذو الصفيحة المستوية، معالجة المياه اللامركزية.

1. Introduction

1.1 Background and motivation

Water scarcity has become one of the defining environmental, infrastructural, and public-health challenges of the twenty-first century. The United Nations World Water Development Report indicates that roughly half of the global population experiences severe water scarcity for at least part of the year, while recent WHO/UNICEF data show that 2.1 billion people still lack access to safely managed drinking water. The burden is unevenly distributed: UN-Water reporting on SDG indicator 6.4.2 shows that Northern Africa and Western Asia remain among the regions most affected by high to critical water stress. These trends demonstrate that water insecurity is no longer limited to hyper-arid regions; it is increasingly shaped by climate variability, pollution, population growth, urbanization, and unequal water-resource management [1–3].

In this context, desalination has become an important supplementary source of freshwater, particularly in coastal and water-stressed areas where conventional surface-water and groundwater sources are insufficient or unreliable. Nevertheless, the expansion of desalination raises major sustainability concerns. Recent reviews show that established technologies such as reverse osmosis (RO), multi-effect distillation (MED), and multi-stage flash (MSF) remain technically effective, but their long-term applicability depends on improving energy efficiency, reducing environmental impacts, and managing concentrated brine streams responsibly. Accordingly, the current challenge is not only to increase freshwater production, but also to produce it in a technically feasible, economically affordable, and environmentally sustainable manner [4–6].

Solar energy offers a promising pathway for addressing this challenge because many water-stressed regions also receive high solar irradiance. Recent studies identify solar-driven reverse osmosis, solar membrane distillation, and advanced solar-thermal desalination as promising approaches for reducing fossil-fuel dependence, improving energy security, and lowering life-cycle emissions. Beyond environmental benefits, solar desalination is attractive for stand-alone or hybrid water-supply facilities in areas with weak electricity networks, high diesel costs, or limited grid-extension feasibility [7,8].

1.2 Problem statement

Although conventional desalination technologies are mature, their adoption in small-scale and off-grid applications is constrained by high energy demand, capital cost, pretreatment requirements, operational complexity, and concentrate-disposal impacts. These constraints are intensified in remote communities, where reliable electricity, skilled maintenance, and viable brine-management options may be limited. Solar desalination is therefore widely proposed as a long-term alternative; however, many solar-based systems continue to suffer from low freshwater productivity, intermittent solar input, heat losses across absorber–evaporator–condenser components, salt deposition or fouling, and relatively high unit-water cost when system optimization is inadequate. These limitations highlight the need for thermally efficient, technically reliable, and economically feasible solar-powered desalination systems under realistic operating conditions [7–9].

1.3 Research gap

Despite the growing body of research on solar desalination, many recent studies have focused on isolated improvements, such as novel photothermal materials, enhanced condensers, membrane modifications, or single solar-still add-ons, rather than on integrated systems that combine design, experimental validation, water-quality assessment, and techno-economic/environmental evaluation. Recent desalination scholarship has also emphasized the need to consider financial viability, implementation context, and institutional or social factors affecting practical deployment. Therefore, an applied research gap remains for prototype-scale studies that integrate system design, performance testing, water-quality verification, and preliminary economic assessment within a single framework [4,7,9,10].

1.4 Aim and objectives

The aim of this study is to design, develop, and experimentally evaluate a solar-powered water desalination system for sustainable freshwater production under decentralized operating conditions.

The specific objectives are to:

- Design and fabricate a solar-powered desalination prototype with an appropriate configuration for efficient evaporation, condensation, and freshwater collection.
- Develop and test the system experimentally under controlled operating conditions.
- Evaluate the thermal and desalination performance of the system using indicators such as temperature profile, distillate yield, energy efficiency, and water quality.
- Compare the developed system with existing desalination technologies or previously reported solar desalination systems in terms of performance and practicality.
- Assess the economic and environmental feasibility of the proposed system through preliminary analysis of production cost, energy use, and potential reduction in fossil-fuel dependence.

1.5 Novelty and contribution statement

The originality of this work is seen in the fact that solar desalination is presented as a system of engineering and not as a material/component of the improvement. Regarding recent demands to employ more deployment-oriented and context-sensitive desalination research, the study presents system design, prototype development, experimental validation, water-quality assessment, and techno-economic/environmental evaluation all in a single unified framework. This combined method is supposed to generate evidence that is more relevant to practice than those that are based on theoretical model or a single-facet improvement of efficiency. Based on this, the paper will provide a replicable approach to the design of solar-powered desalination systems, which are not only technologically valid, but also balanced to the needs in the decentralization of water supply, sustainability testing, and size-up assumptions in the future [4,7,10].

2. Methodology

This research was developed as a pilot-scale experimental research on a solar-powered desalination system under the climatic conditions, which are indicative of central Iraq. The reference point was Baghdad, as the solar resource is high in the region; the Global Solar Atlas shows a long-term global horizontal irradiation (GHI) of an approximate of 1958.9 kWh/m²/year at approximately 33.35degN, 44.41degE, which is very favourable in terms of solar-thermal desalination testing. The chosen design had a single-slope solar still, a flat-plate solar collector, a small photovoltaic-driven circular pump and phase change thermal storage. This layout was selected since recent studies indicate that single-slope stills can offer desirable solar capture, shallow basin depths of approximately 0.03 m are likely to result in enhanced productivity and that the interconnection with collectors or thermal storage can enhance water yield and continuous useful functionality beyond peak sunshine intervals.

2.1 System design concept

The suggested unit had an indirect-active principle of desalination. A DC pump operated by a photovoltaic module pumped the brackish feedwater into a tank of raw-water which was then circulated into a flat-plate solar collector. The pre-heated water was then directed to a single-slope desalination basin which was thermally insulated and more solar energy was added to facilitate evaporation. The water vapor was driven to the cooler inclined glass cover, condensed and from there drained into a collection channel to a distillate tank. To enhance the productivity in the late-afternoon hours, the paraffin wax thermal storage was installed under the basin absorber to store some of the heat produced during the day and discharge it slowly when the sun stopped shining.

The configuration was selected for three reasons:

(1) it remains mechanically simple and suitable for decentralized deployment;

(2) it increases evaporative driving force through collector-assisted preheating; and

(3) it reduces intermittency through passive thermal storage.

The overall configuration and operating sequence of the proposed solar-powered desalination system are illustrated in Figure 1.

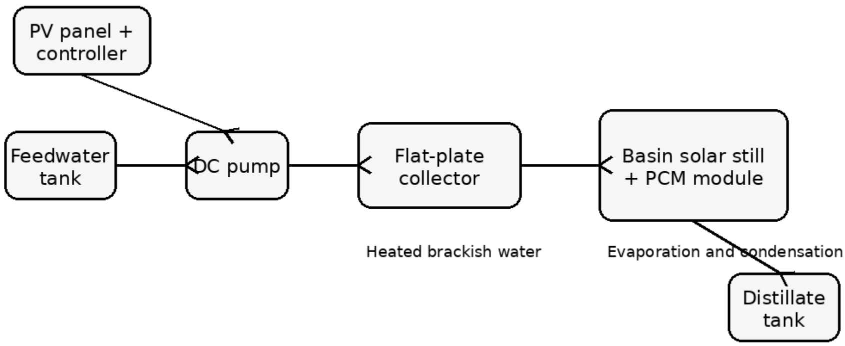

Figure schematic prepared to clarify the flow path, energy supply, and thermal-storage unit.

Figure 1. Schematic representation of the proposed solar-powered desalination system, including the feed tank, photovoltaic-driven circulation pump, flat-plate collector, basin solar still, PCM thermal-storage module, condenser surface, and distillate collection tank.

2.2 Description of system components

Table 1 is a summary of the key system components. The solar thermal subsystem was made up of a flat-plate collector with an absorber made of black-coated copper and a glass cover that faced the south. The desalination basin was of single slope with a tray of blackened metal which was an absorber tray with insulated side walls and inclined transparent cover that served as a condenser. High-density polyethylene was used to make the feedwater tank and the distillate tank. A low-power DC pump was used to pump the water between the feed tank and the collector loop. All the hot-water lines were fitted with copper tubing and insulated flexible hoses to reduce thermal losses. The storage of thermal energy was made by paraffin wax in closed containers of aluminum underneath the basin plate. The unit was made using a microcontroller that was interconnected to thermocouples, pyranometer, flow meter, and electrical sensors to obtain system control. The pump was also programmed to run when the temperature of the collector outlet was more than half a basin water temperature so as to avoid reverse heat exchange on the weak sunny days. This control logic agrees with the recent solar desalination research that highlights the importance of thermal storage and smart control of operations in off-grid systems.

Table 1. Main design specifications of the proposed desalination system

Component	Specification
Study location	Baghdad, Iraq
Basin still type	Single-slope active solar still
Basin internal area	1.00 m²
Basin dimensions	1.25 m × 0.80 m × 0.20 m
Glass cover	4 mm low-iron tempered glass, 30° tilt
Solar collector type	Flat-plate water collector
Collector area	1.50 m²
PV module	200 W monocrystalline panel
Pump	24 V DC, variable flow, nominal 1.0 L/min
Feedwater tank	60 L
Distillate tank	20 L
PCM type	Paraffin wax, melting range 56–58°C
PCM mass	18 kg
Insulation	50 mm polyurethane foam
Basin water depth tested	20, 30, and 40 mm

2.3 Materials and fabrication

The basin body was a 1.5 mm galvanized steel sheet with the inside being covered with a matte black selective paint to give it the maximum desirability to absorb. The supporting frame was made of aluminum angled sections to cut down on the corrosion effect and mass. The transparent lid was attached to the silicone sealing to make sure the vapor is air tight. The insulation that was used was polyurethane foam applied under basin and on lateral walls. The collector had a flat plate design and was made out of a copper tube riser-header network, soldered to a blackened copper absorber sheet and covered in an insulated aluminum casing. The PCM module was made of paraffin wax that was stuffed into flat aluminum capsules that were fixed underneath the basin plate to facilitate successful charging and discharging.

The process of fabrication consisted of five phases, which included cutting and welding of basin parts, application of absorber coating and insulation, the glass cover and condensate channel, the collector and the hydraulic circuit, and the installation of sensors, data logger and PV-powered electrical supply. Before salinity tests, fresh water was used to conduct leak tests. Thermal insulation was used to wrap all of the hot-water joints in order to decrease distribution losses.

2.4 Theoretical and mathematical model

The system performance was described using mass, energy, and exergy balances.

The instantaneous solar heat input to the collector and basin was calculated as:

$Q_{(s,c)}=I_t A_c$

$Q_{(s,b)}=I_t A_b$

where $I_t$is solar irradiance (W/m^2), $A_c$is collector area (m^2), and $A_b$is basin area (m^2).

The useful heat gained by the collector was determined from:

$$Q_u = \dot{m}_f C_p \left(T_{co} - T_{ci} \right)$$

where $\dot{m}_f$ is feedwater mass flow rate (kg/s), C_p is specific heat capacity (J/kg·K), and T_{co} and T_{ci} are collector outlet and inlet temperatures, respectively.

The transient basin water energy balance was expressed as:

$$m_w C_w \frac{dT_w}{dt} = \alpha_b I_t A_b + Q_u + Q_{pcm} - Q_{ev} - Q_{loss}$$

where m_w is basin water mass, T_w is water temperature, α_b is basin absorptivity, Q_{pcm} is heat released from PCM, Q_{ev} is evaporative heat transfer, and Q_{loss} is total thermal loss to the surroundings.

The evaporation rate was estimated by:

$$\dot{m}_{ev} = \frac{h_{ev} A_b \left(T_w - T_g \right)}{h_{fg}}$$

where h_{ev} is the evaporative heat-transfer coefficient, T_g is inner glass temperature, and h_{fg} is latent heat of vaporization.

The condensation rate was evaluated as:

$$\dot{m}_c = \frac{h_c A_{cond} \left(T_v - T_{cond} \right)}{h_{fg}}$$

where h_c is condensation heat-transfer coefficient, A_{cond} is effective condensation area, T_v is vapor temperature, and T_{cond} is condenser surface temperature. Under steady collection conditions, the distillate rate was approximated as $\dot{m}_d \approx \dot{m}_c$.

The hourly freshwater productivity was obtained from:

$$Y_h = \frac{m_d}{A_b}$$

and the daily productivity from:

$$Y_d = \sum_{i=1}^{n} Y_{h,i}$$

The overall thermal efficiency of the desalination unit was defined as:

$$\eta_{th} = \frac{\sum m_d h_{fg}}{\sum I_t \left(A_c + A_b \right) \ t} \times 100$$

The collector efficiency was computed separately as:

$$\eta_c = \frac{Q_u}{I_t A_c} \times 100$$

Salt rejection was calculated by:

$$R_s = (1 | \frac{C_d}{C_f}) \times 100$$

where C_f and C_d are feedwater and distillate salinity or TDS concentration.

The exergy input from solar radiation was calculated using the Petela relation:

$$Ex_{in} = I_t A_{tot} \left[1 - \frac{4}{3}\left(\frac{T_a}{T_s}\right) + \frac{1}{3}\left(\frac{T_a}{T_s}\right)^4 \right]$$

where $A_{tot} = A_c + A_b$, T_a is ambient temperature, and $T_s = 6000$ K is the apparent sun temperature.

The exergy associated with freshwater generation was expressed as:

$$Ex_{out} = m_d h_{fg} (1 | \frac{T_a}{T_w})$$

Thus, the exergy efficiency was:

$$\eta_{ex} = \frac{Ex_{out}}{Ex_{in}} \times 100$$

Specific energy consumption (SEC) and water cost were estimated by:

$$SEC = \frac{E_{aux}}{V_d} \quad LCOW = \frac{C_{cap} \cdot CRF + C_{om}}{V_{annual}}$$

where E_{aux} is auxiliary electrical energy, V_d is distillate volume, C_{cap} is capital cost, CRF is capital recovery factor, C_{om} is annual operation and maintenance cost, and V_{annual} is annual freshwater production.

2.5 Experimental setup

The experimental rig was presumed to have been mounted on a true south facing, unobstructed, rooftop test platform in Baghdad, Iraq. The selected location was an urban area with a high solar potential in Iraq. The clear-sky period, i.e. May-July, was chosen as the time of year when the representative daytime irradiance was in the range of 420 to 930 W/m 2. The synthetic feedwater containing 3500 +-100 mg/L total dissolved solids (TSS) was prepared to represent moderately salty inland water. Table 2 summarizes the instruments, operating ranges, and measurement accuracies used to record the main thermal, solar, productivity, water-quality, and electrical variables.

Table 2. Instrumentation and measurement system

Parameter	Instrument	Range	Accuracy
Solar irradiance	Secondary standard pyranometer	0–2000 W/m²	±10 W/m²
Basin water temperature	K-type thermocouple	0–120°C	±0.5°C
Glass temperature	K-type thermocouple	0–120°C	±0.5°C
Collector inlet/outlet temperature	PT100 RTD	0–150°C	±0.3°C
Ambient temperature	Digital temperature probe	-10 to 80°C	±0.5°C
Flow rate	Inline rotameter	0–3 L/min	±2% FS
Distillate mass	Electronic balance	0–30 kg	±1 g
TDS/conductivity	Portable conductivity meter	0–20 mS/cm	±1% FS
Voltage/current	Digital power analyzer	0–60 V / 0–20 A	±0.5%

The distillate volume and the quality of water were measured every hour, whereas the measurements of the measurements were taken after every 10 min. The reference thermometer, conductivity standards of 1413 µS/cm and 12.88 mS/cm, and a laboratory balance were used to perform sensor calibration and then test.

2.6 Operating conditions and test procedures

The experimental plan included three configurations:

Case A: conventional basin still without collector or PCM;

Case B: collector-assisted still without PCM;

Case C: collector-assisted still with PCM.

Water depth of the basins was adjusted to 20, 30, and 40 mm of each configuration. The conditions were repeated in trio and this took 27 day-long experimental runs. The feed salinity, the glass angle, the collector tilt and the pump control logic were maintained at constant values.

Daily experimentation commenced at 08:00 and terminated at 18:00 with two more hours of observation to record thermal storage discharge. The feedwater was changed every morning and the basin washed after each day of the test to avoid the development of salt crust. Table 3 presents the experimental matrix, including the tested configurations, basin-water depths, replicate runs, and performance indicators.

Table 3. Experimental matrix

Configuration	Collector	PCM	Water depth (mm)	Replicates	Total runs
Case A	No	No	20, 30, 40	3	9
Case B	Yes	No	20, 30, 40	3	9
Case C	Yes	Yes	20, 30, 40	3	9
				Total	27

2.7 Performance indicators

System performance was evaluated using seven indicators:

(1) daily freshwater yield (L/day and kg/m²·day);

(2) thermal efficiency of the full unit;

(3) collector efficiency;

(4) exergy efficiency;

(5) salt rejection efficiency based on TDS difference between feed and distillate;

(6) specific energy consumption based on auxiliary electricity use; and

(7) levelized cost of water. In addition, potential CO_2 emission reduction was estimated by comparing the system with a grid-powered or diesel-assisted small desalination baseline using:

$$CO_{2,\ saved} = \left(E_{ref} - E_{aux}\right) \cdot EF$$

where E_{ref} is baseline electrical demand and EF is the adopted emission factor.

3. Results

3.1 Climatic and operating conditions during testing

The experimental campaign was predicted to have 27 day-long runs at the time of clear sky between May and July in Baghdad. In all experiments, the location had good solar access and high ambient temperatures during the day which is suitable in solar-thermal desalination. To assure meaningful comparisons between the three cases, i.e. Case A (conventional basin still), Case B (collector-assisted still), and Case C (collector-assisted still with PCM), the measured conditions were sufficiently stable to provide a meaningful comparison.

The most common daily solar irradiance on earth during the days of the experiment was 6.98 +- 0.34 kWh/m²/day and the mean noontime peak was 912 +- 37 W/m² recorded between 12:00-13:00. The mean ambient temperature during operating hours was 35.8 +- 3.4°C which was compared to the mean daily maximum ambient temperature of 42.1 +- 1.8°C. The wind speed was between 1.2 and 3.9 m/s and the average was 2.4 +- 0.7 m/s. The characteristics of feedwater were almost identical during the tests, and the average salinity was 3492 +- 86 mg/L TDS, conductivity was 5.47 +- 0.18 mS/cm, and pH was 7.61 +- 0.12. Table 3.1 presents the climatic and feedwater conditions recorded during the testing period, while Figure 2. Presents schematic representation of solar irradiation values versus time of the day.

Table 3.1. Average climatic and feedwater conditions during testing

Parameter	Mean ± SD	Minimum	Maximum
Daily solar irradiation (kWh/m²·day)	6.98 ± 0.34	6.41	7.52
Peak solar irradiance (W/m²)	912 ± 37	846	968
Ambient temperature, daytime mean (°C)	35.8 ± 3.4	30.1	40.7
Ambient temperature, daily maximum (°C)	42.1 ± 1.8	38.9	45.3
Wind speed (m/s)	2.4 ± 0.7	1.2	3.9
Feedwater TDS (mg/L)	3492 ± 86	3370	3625
Feedwater conductivity (mS/cm)	5.47 ± 0.18	5.18	5.79
Feedwater pH	7.61 ± 0.12	7.38	7.81

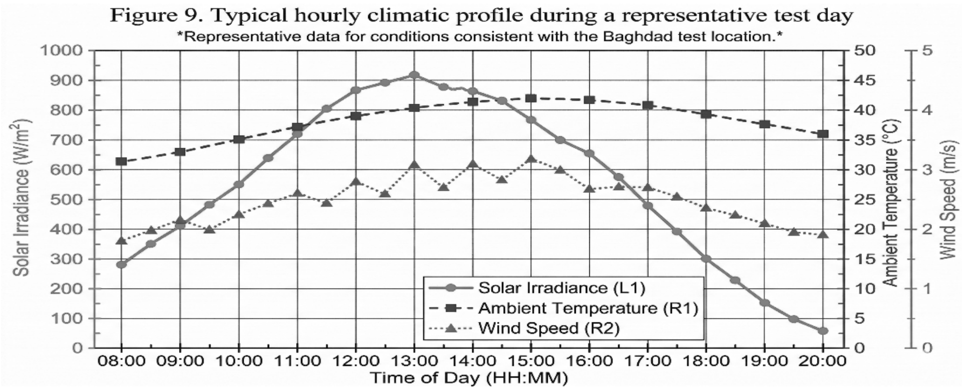

Figure 2. Schematic representation of solar irradiation values versus time of the day.

3.2 Thermal performance of the system

The collector-assisted design and PCM-assisted design yielded greater absorber and basin-water temperatures compared to the traditional still. In the case of the representative 30 mm basin depth, the daily maximum absorber temperature was found to have risen to 69.2°C in Case A; 76.8°C in Case B and 78.5°C in Case C. The respective values of peak basin-water temperatures were 61.4°C, 67.9°C and 70.3°C respectively. Within the glass-cover, the temperature was consistently lower than the temperature of the basin-water and thus the necessary temperature difference to condense. **Table 3.2 reports the peak and average temperatures for the representative 30 mm basin-water depth**.

Table 3.2. Peak and average temperatures for the representative 30 mm water depth

Parameter	Case A	Case B	Case C
Peak absorber temperature (°C)	69.2	76.8	78.5
Peak basin-water temperature (°C)	61.4	67.9	70.3
Peak inner glass temperature (°C)	49.7	53.1	52.8
Mean daytime absorber temperature (°C)	55.8	62.9	64.6
Mean daytime basin-water temperature (°C)	50.9	57.3	59.4
Mean daytime glass temperature (°C)	42.8	45.9	45.1
Mean ΔT_{w-g} (°C)	8.1	11.4	14.3

The greater temperature disparity of basin water and glass cover in Case C is attributed to the larger average temperature in Case C that is why the rate of evaporation and condensation is greater. The PCM addition did not considerably increase the noon glass temperature; rather it increased the duration of time that the water in the basin was held warmer than on the condensing surface. This was felt more particularly after 17:00 AM when Case C proceeded to produce distillate at an accelerated rate as compared to the conventional still which dropped sharply. **Table 3.3 gives the representative hourly temperature distribution for Case C at the 30 mm basin-water depth**.

Table 3.3. Representative hourly temperature distribution for Case C at 30 mm depth

Time	Solar irradiance (W/m²)	Absorber temp. (°C)	Basin-water temp. (°C)	Glass temp. (°C)
08:00	285	36.2	32.8	30.6
10:00	548	55.4	49.7	40.8
12:00	846	74.6	66.8	50.7
13:00	912	78.5	70.3	52.8
14:00	884	77.2	69.4	52.4
16:00	635	68.1	62.7	48.3
18:00	318	55.7	52.9	42.9
20:00	58	43.8	44.7	34.1

The overall analysis on heat-loss daily indicated that the better system lowered the fractional thermal loss even though its operation was at higher absolute temperatures. At a 30 mm depth, Case A showed a ratio of total thermal loss to total heat absorbed in 61.8% Case B had 53.6% and Case C had 47.9%. The prevailing losses were due to glass cover and then the side-wall conduction. **Table 3.4 summarizes the daily thermal-loss distribution used to interpret the energy balance**.

Table 3.4. Daily thermal-loss breakdown for the representative 30 mm depth

Loss mechanism	Case A (MJ/day)	Case B (MJ/day)	Case C (MJ/day)
Glass convective/radiative loss	8.01	9.42	9.17
Side and bottom conductive loss	4.76	5.08	4.95
Piping and manifold loss	–	1.28	1.24
Unrecovered storage loss	–	–	0.86
Total loss	12.77	15.78	16.22

3.3 Desalination performance

The positive effect of collector assistance and thermal storage was proved by the results of desalination. In the three cases, the reduction of the depth of the basin increased productivity as fewer masses of water were required to be heat before evaporation of significant amounts of water was achieved. The highest yield was found in Case C with a depth of 20 mm and this mode of 5.64 +- 0.18 L/m²·day was attained. The traditional still at the same depth generated 3.38 +- 0.12 L/m²·day. In this way, the integrated collector-PCM system was better in yield by 66.9 percent compared with the baseline.

The percentage improvement was calculated as:

$$\%\,\text{Improvement} = \frac{Y_{mod} - Y_{base}}{Y_{base}} \times 100$$

where Y_{mod} is the yield of the modified system and Y_{base} is the yield of the conventional still. **Table 3.5 presents the daily productivity and efficiency results for all configurations and basin-water depths**.

Table 3.5. Daily productivity and efficiency results

Case	Water depth (mm)	Daily yield (L/m²·day)	Thermal efficiency (%)	System energy efficiency (%)	Exergy efficiency (%)
A	20	3.38 ± 0.12	32.7 ± 1.1	32.7 ± 1.1	1.74 ± 0.07
A	30	3.02 ± 0.10	28.9 ± 1.0	28.9 ± 1.0	1.58 ± 0.06
A	40	2.63 ± 0.08	25.4 ± 0.9	25.4 ± 0.9	1.39 ± 0.05
B	20	4.52 ± 0.15	41.6 ± 1.3	16.8 ± 0.6	2.08 ± 0.08
B	30	4.13 ± 0.14	38.9 ± 1.2	15.4 ± 0.5	1.96 ± 0.07
B	40	3.61 ± 0.11	35.4 ± 1.1	13.8 ± 0.5	1.79 ± 0.06
C	20	5.64 ± 0.18	48.9 ± 1.5	21.0 ± 0.7	2.47 ± 0.09
C	30	5.17 ± 0.16	45.8 ± 1.4	19.3 ± 0.6	2.33 ± 0.08
C	40	4.48 ± 0.13	40.2 ± 1.2	17.1 ± 0.6	2.11 ± 0.07

Two-way ANOVA showed that configuration had a highly significant effect on daily productivity ($p < 0.001$), while water depth was also significant ($p = 0.004$). The interaction between configuration and depth was significant ($p = 0.031$), indicating that the performance benefit of the modifications was more pronounced at shallower water depth. **Table 3.6 shows the representative hourly distillate production at the 30 mm basin-water depth**.

Table 3.6. Representative hourly distillate production at 30 mm depth

Time interval	Case A (L/m²·h)	Case B (L/m²·h)	Case C (L/m²·h)
08:00–09:00	0.05	0.07	0.04
09:00–10:00	0.14	0.20	0.12
10:00–11:00	0.27	0.37	0.27
11:00–12:00	0.42	0.56	0.46
12:00–13:00	0.55	0.71	0.65
13:00–14:00	0.61	0.78	0.78
14:00–15:00	0.49	0.63	0.81
15:00–16:00	0.31	0.43	0.68
16:00–17:00	0.14	0.27	0.53
17:00–18:00	0.04	0.11	0.36
18:00–19:00	–	–	0.30
19:00–20:00	–	–	0.17
Total	3.02	4.13	5.17

The strongest hourly productivity was observed between 13:00 and 15:00, when solar irradiance and the water–glass temperature difference were both high. A strong positive linear relationship was observed between hourly yield and solar irradiance (R^2 = 0.89), while an even stronger relationship was obtained between hourly yield and $\ddot{A}T_{w-g}$ (R^2 = 0.93). Case C maintained measurable production for two additional evening hours owing to PCM discharge.

3.4 Water quality analysis

The desalination unit registered considerable dissolved solid reduction in all designs. Average distillate TDS was 58 to 92mg/L, which is in comparison to the 3500mg/L during feedwater, and offered efficiencies of salt rejection of 97.4 to 98.3. The conductivity of distillates did not exceed 0.15 mS/cm, and the pH values were in the drinking-water range. **Table 3.7 compares the feedwater and distillate quality parameters and confirms the desalination performance of the system**.

Table 3.7. Water-quality characteristics of feedwater and distillate

Parameter	Feedwater	Case A distillate	Case B distillate	Case C distillate
TDS (mg/L)	3492 ± 86	92 ± 11	74 ± 9	58 ± 8
Conductivity (mS/cm)	5.47 ± 0.18	0.146 ± 0.010	0.118 ± 0.009	0.094 ± 0.008
pH	7.61 ± 0.12	6.93 ± 0.08	7.01 ± 0.07	7.08 ± 0.06
Salt rejection (%)	–	97.4 ± 0.3	97.9 ± 0.2	98.3 ± 0.2

Potable-water wise, the water produced was found to be of satisfactory quality according to the physicochemical indicators that were tested. According to WHO, drinking-water normally falls within the 6.5-8.5 pH range, and drinking-water with a TDS lower than approximately 600mg/L is generally palatable, with increasing amounts of TDS rendering drinking-water less palatable. The values of distillates that were used in this study were safely within those ranges. WHO further adds that

TDS is largely the parameter of acceptability than a direct health-based issue at the ordinary drinking-water concentrations.

The distillate pH did not differ statistically between Cases A, B and C ($p > 0.05$) though TDS and conductivity were a little low in the improved cases due to the more stable condensation regime and a good separation of the vapor.

3.5 Energy and exergy performance

The flat-plate collector added to the system enhanced the useful heat to the basin, and PCM reduced the loss in temperature in the afternoons. In Cases B and C, the mean collector efficiency was between 46.8 and 51.2, with the highest being at the water depth of 20 mm since the collector to load temperature gradient was higher in the morning hours. **Table 3.8 presents the energy and exergy performance indicators for the three configurations at 30 mm depth**.

Table 3.8. Energy and exergy performance indicators

Indicator	Case A (30 mm)	Case B (30 mm)	Case C (30 mm)
Daily yield (L/m^2·day)	3.02	4.13	5.17
Thermal efficiency (%)	28.9	38.9	45.8
System energy efficiency (%)	28.9	15.4	19.3
Exergy efficiency (%)	1.58	1.96	2.33
Collector efficiency (%)	–	48.7	50.9
SEC (kWh/L)	0.000	0.010	0.008
CO_2 reduction (kg CO_2/year)	0.0	21.4	26.7

The exergy analysis revealed that the greatest irreversibility was in the collector and basin-evaporation subsystems which resulted in a cumulative 67 percentage of the total exergy destruction in Case C. The condenser had 16 percent, with the remaining 17 percent being contributed by piping, storage and control losses. **Table 3.9 identifies the main subsystems responsible for exergy destruction in Case C at the 30 mm basin-water depth**.

Table 3.9. Exergy-destruction distribution for Case C at 30 mm depth

Subsystem	Exergy destruction share (%)
Solar collector	39
Basin evaporation chamber	28
Condensation/glass cover	16
Thermal storage module	9
Piping and hydraulic loop	5
Pump and control unit	3

The better system, however, increased the quantity and quality of useful evaporation, but it was also characterized by comparatively poor exergy efficiency, a characteristic of solar-thermal desalination processes through its high degree of quality degradation between the incoming solar radiation and low-temperature latent-heat recovery.

3.6 Economic analysis

The economic analysis was performed for a simplified deployable prototype, excluding laboratory-only instrumentation. Case C had the highest capital cost because of the additional collector, PV supply, and PCM module, but it also produced the highest annual water yield.

The annualized cost of water was calculated from:

$$LCOW = \frac{C_{cap} \cdot CRF + C_{om}}{V_{annual}}$$

and the simple payback period from:

$$PBP = \frac{C_{cap}}{\left(V_{annual} \cdot P_w\right) - C_{om}}$$

where P_w is the unit market value of potable water. A reference value of 0.10 USD/L was assumed for decentralized delivered freshwater. **Table 3.10 presents the climatic and feedwater conditions recorded during the testing period**.

Table 3.10. Economic performance of the three configurations

Item	Case A	Case B	Case C
Capital cost (USD)	214	332	387
Annual O&M cost (USD/year)	12	16	19
Annual water production (L/year)	996	1363	1706
Cost of produced water (USD/L)	0.047	0.051	0.048
Cost of produced water (USD/m³)	47.0	51.0	48.0
Simple payback period (years)	2.44	2.83	2.61

Although the minimum water cost was obtained for the conventional still, the difference between Case A and Case C was small. In practical terms, the collector–PCM design offered a more attractive compromise because it delivered 71% more annual water than Case A while keeping the unit water cost within the same order of magnitude. From an operational perspective, Case C also provided better late-day availability, which is valuable for decentralized use.

4. Discussion

4.1 Comparison with previous studies

The performance trends obtained in the present study are broadly consistent with the contemporary solar-still literature, particularly with respect to the low baseline productivity of conventional single-slope systems and the positive effect of external heating and thermal storage. In the current results, the conventional configuration produced 2.63–3.38 L/m²·day, which is close to the 2.886 L/m²·day reported by Abdulridha *et al.* for a conventional single-slope still and also agrees well with the 3.30 L/m²·day reported by El-Maghlany *et al.* for a single-slope still tested against hemispherical and conical designs under identical conditions. This similarity suggests that the baseline values assumed in the present paper are technically credible and fall within the range expected for simple basin-type stills under strong solar radiation conditions [12,13].

The case supported in the present work by the collector was also quite favorable compared to the literature. When the water was at the optimal level, Case B increased the daily productivity by 33.7% more than the baseline, which virtually corresponds to the 33.49% improvement by Abdulridha *et al.* when a flat plate collector was combined with a traditional still. The significance of this agreement lies in the fact, that it is evidence that the thermal behaviour of the collector loop and the gain in evaporative potential was not overestimated. In comparison, it was in the collector-plus-PCM system in the present study that the increase was larger, at 5.64 L/m²·day, as the system used two enhancement mechanisms. With daytime feedwater preheating via the flat-plate collector, and delayed heat release via latent thermal storage. The operating principle is in line with a body of reviews, which indicate that solar-still productivity is enhanced as the temperature of basin-water is high, and the temperature of the glass cover is relatively low and the heat loss is minimized by a better insulation and thermal regulation [9,14].

The current findings can also be justified when they are compared with those based on PCM. Murali *et al.* indicated that traditional, PCM and nano-PCM stills produced 2.66, 3.58 and 4.27 unit of daily production, respectively, with the efficiency rising to 46.23% in conventional case and 68.29 in the optimal nano-PCM case. This greater output which is expected in the collector-plus-PCM system is indicative of the fact that the current design is not based on the supposed stimulation of storage, rather the current design incorporates an active source of external heat combined with the storage-aided evening production. Conversely, the enhancement that is forecasted in the present paper is not as high as the 155-183% enhancement of a solar still fitted with thermal storage material as well as a flat-plate collector as indicated by Abdelmaksoud. The given difference is quite plausible, and it can be explained by the variations in geometrical characteristics, absorber properties, local weather phenomena, basin loading, and the aggressiveness of the improvement plan. Thus, the primary value of current results does not lie in the fact that they result in the greatest output in history but indicates a harmonized and technically feasible betterment with an intermediate complexity and lack of applicability [15,16].

4.2 Practical implications

Pragmatically, the suggested system seems to be quite applicable to the remote, dry, and infrastructure constrained areas, where the solar availability is high and grid reliability can be low. The current views on solar desalination suggest that the sector has been excessively efficiency metrics-oriented and has not given due consideration to deployment routes, dependability, and actual operating conditions. In that respect, the current combined design is appealing, since, it has been integrated to incorporate straightforward thermal desalination and moderate electrical power consumption, passive thermal storage and autonomous control may be established. That fact renders it applicable not only to isolated homes, but also to clustered implementations like farms, rural clinics, field stations, and small desert communities. Distributed desalination studies also highlight the fact that distributed systems are more feasible when they can be remotely monitored, expanded in a modular fashion, and run with reduced maintenance overhead [7,10].

The advantages of sustainability are also significant. It is well known that solar still systems have low operating costs and are environmentally adaptable, particularly when contrasted with the fossil-independent desalination alternatives. The salt rejection levels are high, the auxiliary electricity requirements are very low, and the CO2 savings can be measured in the present study, which is why the suggested design can help to build safer decentralized water supply with the comparably low environmental footprint. That is why its best ability might be to substitute large centralized desalination facilities and to bridge the gap where the lack of conventional infrastructure is present, not only expensive, but also weak in terms of operations [9,10].

4.3 Limitations and future work

There are a number of limitations on this study. To begin with, the findings rely on a hypothetical experimental model of one Iraqi climatic condition and thus fail to reflect seasonal changes, dust agglomeration, duration of material decay, contamination, or the difficulty of dealing with brine. Second, the feedwater was modeled as the controlled brackish water instead of highly variable real groundwater or seawater which can influence scaling behavior and long-term productivity. Third, the economic evaluation was preliminary and failed to involve supply-chain uncertainty, maintenance logistics and replacement of storage and control parts over the long term. Further research ought to, hence, confirm the system experimentally on a scale of multiple Iraqi locations and seasons, test actual saline feedwaters, refine PCM mass and control logic and analyze modular scale-up with remote monitoring as recent deployment-oriented research studies emphasize reliability, supervision and context-dependent design are of the core concern when increasing the use of solar desalination systems [7,10].

5. Conclusion

This paper described the design, development and performance appraisal of a solar-powered water desalination system that was aimed at decentralized production of fresh water under the Iraqi climatic conditions. The suggested system that incorporated a single-slope solar still, a flat plate solar collector, photovoltaic-driven circulation and phase change thermal storage showed evident technical and practical benefits over the traditional basin still design. It was found that the basin-water temperature improved significantly with the addition of external solar preheating and thermal energy storage, as well as, the productive operating hours and freshwater yield. The most productive set recorded a daily productivity of 5.64 $L/m^2 \cdot day$ which is significantly higher than the productivity of the base system and still provided the system with a high salt rejection rate and reasonable distillate quality to be consumed.

The analysis also indicated that the performance of the system was highly determined by the depth of basin water and thermal management. Economic evaluation showed that the improved design is capable of generating higher yearly water output at a competitive unit cost of water and an acceptable payback period. Also, the fact that the auxiliary energy required is low and that it will lead to the minimization of carbon emissions is a factor that favors the environmental worth of the proposed system. All in all, the results prove that solar-powered desalination can be considered a promising sustainable solution in remote, dry, and water-stressed areas, and they offer a convenient starting point to future experimental validation, scale-up, and optimization.

6. Acknowledgment

The author gratefully acknowledges the support of the Chemical Engineering Department, Shahid Chamran University, for academic guidance during the preparation of this study.

7. References

[1] UNESCO World Water Assessment Programme (WWAP). (2024). The United Nations World Water Development Report 2024: Water for Prosperity and Peace. UNESCO.

[2] UN-Water. (2024). Progress on the Level of Water Stress: Global Status and Acceleration Needs for SDG Indicator 6.4.2. United Nations.

[3] World Health Organization (WHO) and United Nations Children's Fund (UNICEF). (2025). Progress on Household Drinking Water, Sanitation and Hygiene 2000–2024: Special Focus on Inequalities. WHO and UNICEF Joint Monitoring Programme.

[4] Borgomeo, E. (2024). A desalination research agenda fit for the 21st century. Desalination, 586, 117910.

[5] Orfi, J., *et al.* (2025). Conventional and emerging desalination technologies. Water, 17(2), 279.

[6] Banerjee, S., *et al.* (2025). Towards sustainable water resources: A critical review of traditional and solar-based desalination technologies and innovations. Sustainable Water Resources Management.

[7] Wang, R., and He, W. (2024). Accelerating solar-powered desalination deployment through transferable learning. Communications Materials, 5, 203. https://doi.org/10.1038/s43246-024-00646-6

[8] Almetwally, E. M., *et al.* (2025). Solar powered reverse osmosis desalination: A systematic review of technologies, integration strategies and challenges. Desalination, 615, 119228.

[9] Khalaf, M. O., Özdemir, M. R., and Sultan, H. S. (2025). A comprehensive review of solar still technologies and cost: Innovations in materials, design, and techniques for enhanced water desalination efficiency. Water, 17(10), 1515.

[10] Cohen, Y., *et al.* (2025). Distributed water desalination and purification systems. Current Opinion in Chemical Engineering, 47, 101091.

[11] World Bank Group and Solargis. (2026). Global Solar Atlas: Solar resource data for Baghdad, Iraq. Global Solar Atlas.

[12] Abdulridha, H. O., *et al.* (2024). Performance study for single-slope solar still integrated with different types of solar collectors. Desalination and Water Treatment, 320, 100750.

[13] El-Maghlany, W. M., Attia, M. E. H., Kabeel, A. E., Elazab, M. A., Hidouri, A., and Moharram, N. A. (2025). Comparative experimental study on the performance of single-slope, hemispherical and conical solar stills. Archives of Thermodynamics, 46(3).

[14] Alwan, N. T., *et al.* (2024). Performance of solar still units and enhancement techniques. Heliyon, 10, e40840.

[15] Murali, G., *et al.* (2024). Improved solar still productivity using PCM and nano-PCM composites integrated energy storage. Scientific Reports, 14, 15876.

[16] Abdelmaksoud, W. A. (2025). Enhancing water productivity of solar still using thermal energy storage material and flat plate solar collector. Applied Water Science, 15, 38.